JOURNAL OF GEOPHYSICAL RESEARCH, VOL. ???, XXXX, DOI:10.1029/,

The relationship between the ionospheric eastward electric field and the equatorial electrojet

Patrick Alken

National Geophysical Data Center, NOAA, Boulder, Colorado, USA

Stefan Maus

National Geophysical Data Center, NOAA, Boulder, Colorado, USA

Patrick Alken, National Geophysical Data Center, NOAA E/GC1, 325 Broadway, Boulder, CO 80305-3328, USA. (patrick.alken@noaa.gov)

Abstract. The equatorial electrojet (EEJ) is a strong ionospheric current along the magnetic equator driven by the day side eastward electric field. Current strength is affected by two-stream and gradient-drift instabilities which pose a serious obstacle to quantitative electrodynamic modeling of the equatorial ionosphere. Using highly accurate radar and magnetic field measurements taken over the past decade, we deduce empirical relations between the observed EEJ and the driving eastward electric field. These indicate that the current strength is largely unaffected by instabilities for eastward fields in the range of -0.4 mV/m to 0.07 mV/m. This is followed by a band of moderate current reduction from 0.07 mV/m to 1 mV/m, consistent with predictions for the gradient drift instability. At even stronger eastward fields, a further current reduction is observed, as expected for the two-stream instability. These non-linear empirical relations can be used to correct ionospheric electric field strengths inferred from space and ground-based magnetic field measurements.

1. Introduction

The equatorial electrojet (EEJ) is an intense current system which flows along the magnetic equator in the day-side ionospheric E-region. The neutral wind dynamo drives the EEJ by creating an eastward equatorial electric field (EEF), which sets up a vertical polarization field due to the nonconducting layers above and below the E-region. This vertical electric field drives the equatorial electrojet as an east-west Hall current [*Heelis*, 2004]. The EEJ provides a great deal of information on ionospheric conditions and has been extensively studied for many decades. Early and modern attempts to model the EEJ current system have found discrepancies between theory and observed data. *Gagnepain et al.* [1977] compared early EEJ models with data taken from ground radar, rocket experiments, and ground-based magnetometers, and found that the electron collision frequency had to be enhanced by an ad-hoc factor of 4 to achieve the best agreement with the models. They postulated that this was due to the gradient drift instability, but the exact nature of this mysterious factor 4 has remained unexplained to this day, and modern EEJ modelers continue using it [*Alken and Maus*, 2009; *Fang et al.*, 2008].

There exist two varieties of plasma instabilities in the equatorial electrojet. The type-1 irregularities, also called two-stream instabilities, are excited when the electrons drift through the ions at a velocity exceeding the sound velocity, hence the term "two-stream." Two-stream irregularities are observed during the day and night when the electron drift velocity is somewhat larger than the ion acoustic velocity (about 360 m/s for typical electrojet conditions). Type-2 irregularities, also called gradient drift instabilities, are excited when there exists a large electron density gradient in the $\mathbf{J} \times \mathbf{B}$ direction, in

addition to the electron drift exceeding a certain threshold. Both the type-1 and type-2 instabilities lead to field aligned irregularities in electron density with scale sizes ranging from about a meter to a few kilometers [*Fejer and Kelley*, 1980].

Both types of instabilities reduce the vertical polarization electric field, and hence the EEJ current. To reproduce this reduced current without a full treatment of the physics of the instabilities, modelers simply increase the electron collision frequency in their models by the above mentioned factor 4, which appears to work well. When *Gagnepain et al.* [1977] first studied this effect, they focused on typical EEJ conditions and did not consider westward counter-electrojet (CEJ) events or extreme eastward currents during storm-time conditions. In this study, we provide a more detailed analysis, and show that though the factor 4 enhancement appears to work well for normal day time electric fields, it is not adequate to describe the effects of higher electric field values during storm times, nor does it accurately reflect conditions during westward CEJ electric fields. At high (> 1 mV/m) eastward electric fields, we show that an additional suppression of EEJ current strength occurs, due to the effects of the two-stream instability. Furthermore, the factor 4 enhancement is not applicable for westward and small eastward fields, since the gradient drift instability is not present.

2. Methodology

In order to model the E-region currents and electric fields, we used the method of *Alken and Maus* [2009], which is based on CHAMP satellite magnetometer measurements. The CHAMP (CHAllenging Minisatellite Payload) satellite was launched into a polar circular orbit in July 2000 with an initial altitude of 454 km. CHAMP's inclination of 87.3° enables it to record high-quality latitudinal magnetic profiles of the equatorial electrojet current.

To determine the EEJ current density from the magnetic signature, the POMME-5 [*Maus et al.*, 2006] model was subtracted to eliminate core, mantle, crust, and magnetospheric fields. Then, contributions from the Sq current system are filtered out by fitting and subtracting the background magnetic field. The resulting magnetic profile of the EEJ is inverted for a latitudinal current profile [*Lühr et al.*, 2004]. This 2D observed current profile is modeled by solving the governing electrodynamic equations [*Alken and Maus*, 2009; *Alken*, 2009]. Once the equations are solved using an initial guess of the eastward electric field, the resulting current is compared with corresponding CHAMP satellite measurements, and an electric field estimate is produced which provides the best agreement between the modeled and observed current profiles. This study found that to produce the best agreement between CHAMP electric field estimates and corresponding radar measurements, the conductivity inputs to the electrodynamic equations had to be modified by artificially increasing the electron collision frequency by a factor 4, in accordance with the findings of *Gagnepain et al.* [1977]. The radar measurements were taken by JULIA (Jicamarca Unattended Long-term studies of the Ionosphere and Atmosphere), which is a coherent scatter radar located at the Jicamarca Radio Observatory (JRO) in Peru. JULIA measures plasma drift velocities at 150 km altitude near the dip equator, during the day-time from about 0800 to 1600 local time [*Hysell et al.*, 1997].

A major limitation of this study in further analyzing this factor 4 enhancement was the lack of data for both westward (CEJ) electric fields and high (> 1 mV/m) electric fields (see [*Alken and Maus*, 2009, Fig. 3]), which is due to the limited number of CHAMP satellite passes over the JULIA radar. In order to produce a dataset with better coverage, we turned to the extensive ΔH magnetometer measurements from the Jicamarca and

Piura observatories. It is known that the difference ΔH between a magnetic horizontal intensity measurement taken on the dip equator and a measurement taken a few degrees away from the equator provides an accurate means of monitoring the EEJ strength and has been used to infer F-region vertical drift [*Anderson et al.*, 2004]. Because the method of *Alken and Maus* [2009] relies on a full latitudinal current profile of the EEJ, we used the ΔH measurements taken from Jicamarca (dip latitude 0.8°N) and Piura (dip latitude 6.8°N) from February 1997 through March 2009, as provided by the Jicamarca Radio Observatory, and computed a CHAMP latitudinal current profile, simulating what the CHAMP satellite would have recorded if it had flown over Jicamarca for each ΔH observation. This was done by taking all CHAMP satellite passes within 15° longitude of Jicamarca and computing one current profile, J_{avg}, averaged over all local times and seasons. Then, for each ΔH measurement, we assume that the corresponding current that CHAMP would have measured, had it flown over at that time, is given by

$$J_{\Delta H} = \alpha \Delta H J_{avg} \tag{1}$$

where α is an empirical proportionality constant which provides correct units. This approach assumes that the height-integrated meridional current profile has a unique shape which simply scales with the strength of the electrojet, which is tracked by ΔH. A possible future improvement of the method would be to separately determine representative CHAMP current profiles for different local times and seasons. To determine α, we took individual CHAMP overflights along with the corresponding ΔH and computed

$$\alpha_i = J_i^0 / (J_{avg}^0 \Delta H_i), \tag{2}$$

where J^0 represents the value of the current on the magnetic equator. A histogram was made of the α_i values, and a quantile analysis was performed to determine if the α_i are normally distributed. A plot of normal quantiles versus the α_i quantiles yielded a linear relation with a correlation of 0.97 and a best fit slope of 0.03, indicating that the α_i values come from a linearly transformed normal distribution. Fitting the α_i histogram to a Gaussian function produced a standard deviation of 0.017 nT^{-1} and a mean of 0.050 nT^{-1}, which was taken to be the final value of α. With α determined, a large dataset of simulated current profiles could be computed for more than a decade of ΔH measurements. Each of these current profiles was then inverted for both an eastward and vertical electric field estimate using the method of *Alken and Maus* [2009]. In order to validate this method of converting ΔH observations into latitudinal current profiles, we compared the electric field values obtained from $J_{\Delta H}$ with the corresponding EEF values from individual CHAMP profiles, for all CHAMP passes within 15° longitude of Jicamarca. The CHAMP-derived EEF values have already been validated by *Alken and Maus* [2009] against JULIA radar measurements with a correlation of 0.84 and rms error of 0.13 mV/m when the factor 4 correction was included.

There were a total of 590 CHAMP overflights which had corresponding ΔH observations for the period 2000 - 2009. With and without the factor 4 enhancement of the electron collision frequency, we find a high correlation coefficient of 0.84 between $E_{\Delta H}$ and E_{CHAMP}. Without the correction factor, we find an rms error of 0.07 mV/m. With the factor 4 enhancement, the rms error is 0.14 mV/m. The large dataset of ΔH electric field values provides much of the previously missing information on westward and large eastward electric field events.

3. Results

The JULIA coherent scatter radar at Jicamarca operates during typical day-time conditions and provides a large database of vertical drift measurements at 150 km altitude from which an eastward electric field can be inferred. In order to analyze ultra-high electric field conditions, we turned to the Jicamarca incoherent scatter radar (ISR), which recorded zonal electric fields up to nearly 3 mV/m during the November 2004 super-storm. The 50 MHz incoherent scatter radar at Jicamarca can make highly accurate F-region plasma drift measurements when the transmitting antenna beam is pointed perpendicularly to the geomagnetic field [*Kudeki et al.*, 2003]. We used all available ISR measurements at 300 km altitude in our analysis, except for those recorded on December 16, 2003 and September 13-21, 2005. During these two storms, the ΔH observations from Jicamarca and Piura exhibited large offsets, indicating baseline errors in the magnetometer measurements, and so these data were removed from consideration.

In Fig. 1, we plot the JULIA and ISR electric field data against the ΔH-derived EEF values. We restricted this plot to include only the ISR data from the November 2004 super-storm to avoid too much clutter (the full ISR data set is shown in the next figure). This storm provides zonal electric field measurements up to nearly 3 mV/m. To illustrate the large number of JULIA data, we binned the electric field measurement from JULIA with its corresponding modeled EEF value from $J_{\Delta H}$ into a 2D histogram, using a grid of 0.06 mV/m by 0.06 mV/m, and plotted the density $n(E_{JULIA}, E_{J_{\Delta H}})$ as a color map. In the case of westward fields, we see that the highest density lies along $y = x$ when no correction factor is applied to the electron collision frequency. For eastward fields, the highest density lies along $y = x$ only when the factor 4 enhancement is applied. This

is in agreement with the results of *Alken and Maus* [2009] based on CHAMP magnetic field measurements. The black points show the ISR EEF measurements taken at 300 km altitude. We restricted the ISR measurements to the 10-16 local time sector, since that is when JULIA data is typically available. For both the JULIA and ISR data, the vertical drift measurements were converted to EEF through the standard relation $\mathbf{v} = \mathbf{E} \times \mathbf{B}/B^2$, where $\mathbf{B}$ is the ambient main magnetic field. We see that when no electron collision frequency correction factor is applied, the ISR data also tend to lie along $y = x$ for westward electric fields, but diverge for eastward fields. When the factor 4 correction is applied, the eastward field derived from ISR measurements aligns along $y = x$ except for the ultra high fields, above about 1 mV/m.

In order to quantify these relationships, we sorted the JULIA data into 0.03 mV/m bins and computed means of each bin. The results without and with the factor 4 correction are shown in Figs. 2(a) and (b). The $\pm\sigma$ curves represent the standard deviation of the mean of each bin. Without the correction, the curve lies close to the $y = x$ line for westward fields, and suddenly reduces slope at a small eastward field of about 0.07 mV/m based on visual inspection of the data. With the factor 4 correction applied, we see that the westward fields are no longer inferred accurately, but eastward fields are, with the possible exception of higher fields (> 1 mV/m), though it is difficult to quantify this from the JULIA data alone. In Fig. 2(c), we again show the JULIA curve along with a scatter plot of the Jicamarca ISR data, without applying the factor 4 correction. The ISR data provides coverage up to about 3 mV/m. They confirm the reduction in current for eastward fields. Fig. 2(d) shows the same data with the factor 4 correction applied and we see clearly that at higher fields (> 1 mV/m) there is indeed another reduction

in slope, indicating that a second unmodeled physical mechanism becomes active, further reducing the ability of eastward electric fields to drive the EEJ.

The bottom four plots in Fig. 2 show the same data as the top four, however the y-axis now shows the modeled vertical electric field solution at 105 km altitude. In order to translate the $y = x$ line into these plots, the curve in Fig. 2(e) was divided by the curve in Fig. 2(a), giving an average value of 30. A similar procedure for Figs. 2(f) and (b), yielded an average value of 17. We see the same general features in the vertical electric field plots as in the horizontal electric field plots. We have included the vertical electric field plots since much of the theory of electrojet instabilities is formulated in terms of the vertical field, which is directly proportional to the speed of the electrons which carry the EEJ current. The dashed black lines in these figures represent threshold electric field values which are discussed below.

4. Discussion

Discrepancies between the measured EEF and its prediction from ΔH have been an open question for several decades. *Gagnepain et al.* [1977] first proposed enhancing the electron collision frequency as an empirical solution to this problem, and postulated that the gradient drift instability could be the mechanism responsible for the discrepancies. Their analysis was limited by the available data coverage at that time. The main effect of enhancing the electron collision frequency is to reduce the vertical polarization electric field and hence the predicted EEJ current. *Ronchi et al.* [1990, 1991] examined the effects of including ionospheric instabilities in EEJ models and concluded that the polarization electric field would be significantly reduced, but the exact nature of the factor 4 remained unexplained.

Using the linear theory of equatorial plasma instabilities, the threshold horizontal drift velocity for the gradient drift instability is given by *Fejer et al.* [1975]

$$V_d \geq L_N \left[2\alpha N_0 (1+\psi_0) \frac{\Omega_i}{\nu_i} + \frac{\nu_e k^2 C_s^2}{\nu_i \Omega_e} \right] (1+\psi_0) \tag{3}$$

where ν_e, ν_i, Ω_e, and Ω_i are the electron and ion collision frequencies and gyro-frequencies, N_0 is the electron density, $L_N = N(\partial N/\partial z)^{-1}$ is the vertical electron density gradient length, C_s is the ion acoustic velocity, $\psi_0 = \nu_e \nu_i / \Omega_e \Omega_i$, α is the recombination rate, and k is the horizontal wavenumber of the plasma waves of interest. Using typical day time electrojet region values for these parameters, *Fejer et al.* [1975, pg. 1321] predict the threshold velocity for the gradient drift instability to lie between 32 m/s and 70 m/s, depending on the wavelength of the relevant plasma waves. Taking a typical magnetic field value of about 24750 nT over Jicamarca at 110 km altitude for the years 2000 - 2009, this translates into a vertical electric field ranging from 0.8 mV/m to 1.7 mV/m in the no correction case. We have drawn these two lines on Figs. 2(e),(g) and indeed find that the first change in slope occurs within this range of E_z, confirming the prediction of *Fejer et al.* [1975].

Turning now to the second change in slope at higher fields, we postulate that this could be due to the type-1 E-region plasma instability, known as the two-stream instability. The threshold condition for the horizontal drift velocity required to excite this instability is given by *Kelley* [1989] as

$$V_d \geq (1+\psi_0) C_s, \tag{4}$$

where ψ_0 was defined above. Typically, the ion acoustic velocity C_s in the electrojet region is about 360 m/s. A typical value of ψ_0 is 0.22. This leads to a threshold drift velocity of

440 m/s, or about 10.9 mV/m for the vertical electric field in the no correction case (see also *Hysell et al.* [2007]). Fig. 2(g) includes this threshold line, which indeed corresponds well with the second change in slope at high electric field values.

5. Conclusion

For several decades, equatorial electrojet modelers have known that changes in the E-region eastward equatorial electric field do not have a one-to-one correspondence with changes in the strength of the electrojet current. Historically, modelers have accounted for this using an empirical correction factor for the electron collision frequency. Using a large database of satellite magnetic measurements, ground based radar observations, and ground magnetometer measurements, this study has for the first time shown that the discrepancies between the EEF and corresponding ΔH measurements are due to both type-1 and type-2 ionospheric instabilities. We find that there is a one-to-one correspondence between the EEF and ΔH for nominal westward fields, when neither instability is present. At very small, positive eastward fields we again find a one-to-one correspondence, since the type-2 gradient drift instability typically does not become active until the vertical electric field reaches 0.8 to 1.7 mV/m above Jicamarca. Above this threshold, we find that increases in the EEF do not lead to corresponding increases in ΔH, which is due to the gradient drift instability reducing the vertical polarization electric field and hence the EEJ current. At very high fields, typically above E_z values of 10 - 11 mV/m in the Peruvian sector, the type-1 two-stream instability becomes active, leading to a further reduction in the EEJ current and corresponding ΔH signature. This study has confirmed predictions from linear ionospheric instability theory of the influence of type-1 and type-2

instabilities both on the strength of the EEJ and on the threshold fields required for the instabilities to become active.

There are two possibilities for making higher accuracy EEJ models in the future. The first would be to empirically determine what enhancement factor is needed for any given EEF value, essentially creating a calibration curve input to the model. The second would be to include the physics of both instabilities in the EEJ model equations, eliminating the need for artificially enhancing the electron collision frequency.

Acknowledgments. The Jicamarca Radio Observatory is gratefully acknowledged for providing the JULIA and ISR radar data as well as the ground-based magnetometer data for this study. The Jicamarca Radio Observatory is a facility of the Instituto Geofisico del Peru operated with support from the NSF Cooperative Agreement ATM-0432565 through Cornell University. The Piura magnetic observatory is gratefully acknowledged for providing ground-based magnetometer data. The operational support of the CHAMP mission by the German Aerospace Center (DLR) is gratefully acknowledged. This work was supported by the NASA grant NNX08AG09G.

References

Alken, P. (2009), Modeling equatorial ionospheric currents and electric fields from satellite magnetic field measurements, PhD thesis in Physics, University of Colorado at Boulder.

Alken, P., and S. Maus (2009), Electric fields in the equatorial ionosphere derived from CHAMP satellite magnetic field measurements, *J. Atmos. Sol. Terr. Phys.*, in press.

Anderson, D., A. Anghel, J. Chau, and O. Veliz (2004), Daytime vertical E $\times$ B drift velocities inferred from gound-based magnetometer observations at low latitudes, *Space*

Weather, *2*, S11001, doi:10.1029/2004SW000095.

Buneman, O. (1963), Excitation of field aligned sound waves by electron streams, *Phys. Rev. Lett.*, *10*(7).

Drob, D. P., et al. (2008), An empirical model of the earth's horizontal wind fields: HWM07, *J. Geophys. Res.*, *113*, A12304, doi:10.1029/2008JA013668.

Fang, T. W., A. D. Richmond, J. Y. Liu, A. Maute, C. H. Lin, C. H. Chen, and B. Harper (2008), Model simulation of the equatorial electrojet in the Peruvian and Philippine sectors, *J. Atmos. Sol. Terr. Phys.*, *70*, 2203–2211.

Farley, D. T. (1963), A plasma instability resulting in field-aligned irregularities in the ionosphere, *J. Geophys. Res.*, *68*, 6083.

Fejer, B. G., and M. C. Kelley (1980), Ionospheric irregularities, *Reviews of Geophysics and Space Physics*, *18*(2), 401–454.

Fejer, B. G., D. T. Farley, B. B. Balsley, and R. F. Woodman (1975), Vertical structure of the VHF backscattering region in the equatorial electrojet and the gradient drift instability, *J. Geophys. Res.*, *80*(10), 1313–24.

Forbes, J. M. (1981), The equatorial electrojet, *Reviews of Geophysics and Space Physics*, *19*(3), 469–504.

Gagnepain, J., M. Crochet, and A. D. Richmond (1977), Comparison of equatorial electrojet models, *J. Atmos. Terr. Phys.*, *39*, 1119–1124.

Heelis, R. A. (2004), Electrodynamics in the low and middle latitude ionosphere: a tutorial, *J. Atmos. Sol. Terr. Phys.*, *66*, 825–38.

Hoh, F. C. (1963), Instability of Penning-type discharges, *Phys. Fluids*, *6*(8).

Hysell, D. L., M. F. Larsen, and R. F. Woodman (1997), JULIA radar studies of electric fields in the equatorial electrojet, *Geophys. Res. Lett.*, *24*(13), 1687–90.

Hysell, D. L., J. Drexler, E. B. Shume, J. L. Chau, D. E. Scipion, M. Vlasov, R. Cuevas, and C. Heinselman (2007), Combined radar observations of equatorial electrojet irregularities at jicamarca, *Annales de Geophysicae*, *25*, 457–473.

Kelley, M. C. (1989), *The Earth's Ionosphere: Plasma Physics and Electrodynamics*, Academic Press Inc, San Diego.

Kudeki, E., R. F. Woodman, and Z. Feng (2003), Incoherent scatter radar plasma density measurements at jicamarca using a transverse-mode differential-phase method, *Geophys. Res. Lett.*, *30*(5), doi:10.1029/2002GL015496.

Lühr, H., S. Maus, and M. Rother (2004), Noon-time equatorial electrojet: Its spatial features as determined by the CHAMP satellite, *J. Geophys. Res.*, *109*, A01306, doi: 10.1029/2002JA009656.

Maus, S., M. Rother, C. Stolle, W. Mai, S. Choi, H. Lühr, D. Cooke, and C. Roth (2006), Third generation of the Potsdam Magnetic Model of the Earth (POMME), *Geochem. Geophys. Geosyst.*, *7*, doi:10.1029/2006GC001269.

Richmond, A. D. (1973), Equatorial electrojet - I. Development of a model including winds and electric field, *J. Atmos. Terr. Phys.*, *35*, 1083–1103.

Ronchi, C., R. N. Sudan, and P. L. Similon (1990), Effect of short-scale turbulence on kilometer wavelength irregularities in the equatorial electrojet, *J. Geophys. Res.*, *95*(A1), 189–200.

Ronchi, C., R. N. Sudan, and D. T. Farley (1991), Numerical simulations of large-scale plasma turbulence in the daytime equatorial electrojet, *J. Geophys. Res.*, *96*(A12),

21,263–21,279.

Simon, A. (1963), Instability of a partially ionized plasma in crossed electric and magnetic fields, *Phys. Fluids*, *6*(3).

Sugiura, M., and J. C. Cain (1966), A model equatorial electrojet, *J. Geophys. Res.*, *71*(7), 1869–1877.

Sugiura, M., and D. J. Poros (1969), An improved model equatorial electrojet with a meridional current system, *J. Geophys. Res.*, *74*, 4025–34.

Untiedt, J. (1967), A model of the equatorial electrojet involving meridional currents, *J. Geophys. Res.*, *72*(23).

Figure 1. JULIA (color map) and November 2004 storm time ISR (black) eastward electric field data on horizontal axis. Corresponding modeled eastward electric field value computed from $J_{\Delta H}$ profile on vertical axis. The $y = x$ line is shown in red.

Figure 2. Smoothed JULIA data (150 km altitude) with all ISR scatter data (300 km altitude) for both the EEF and vertical polarization electric field. See text for more detail.

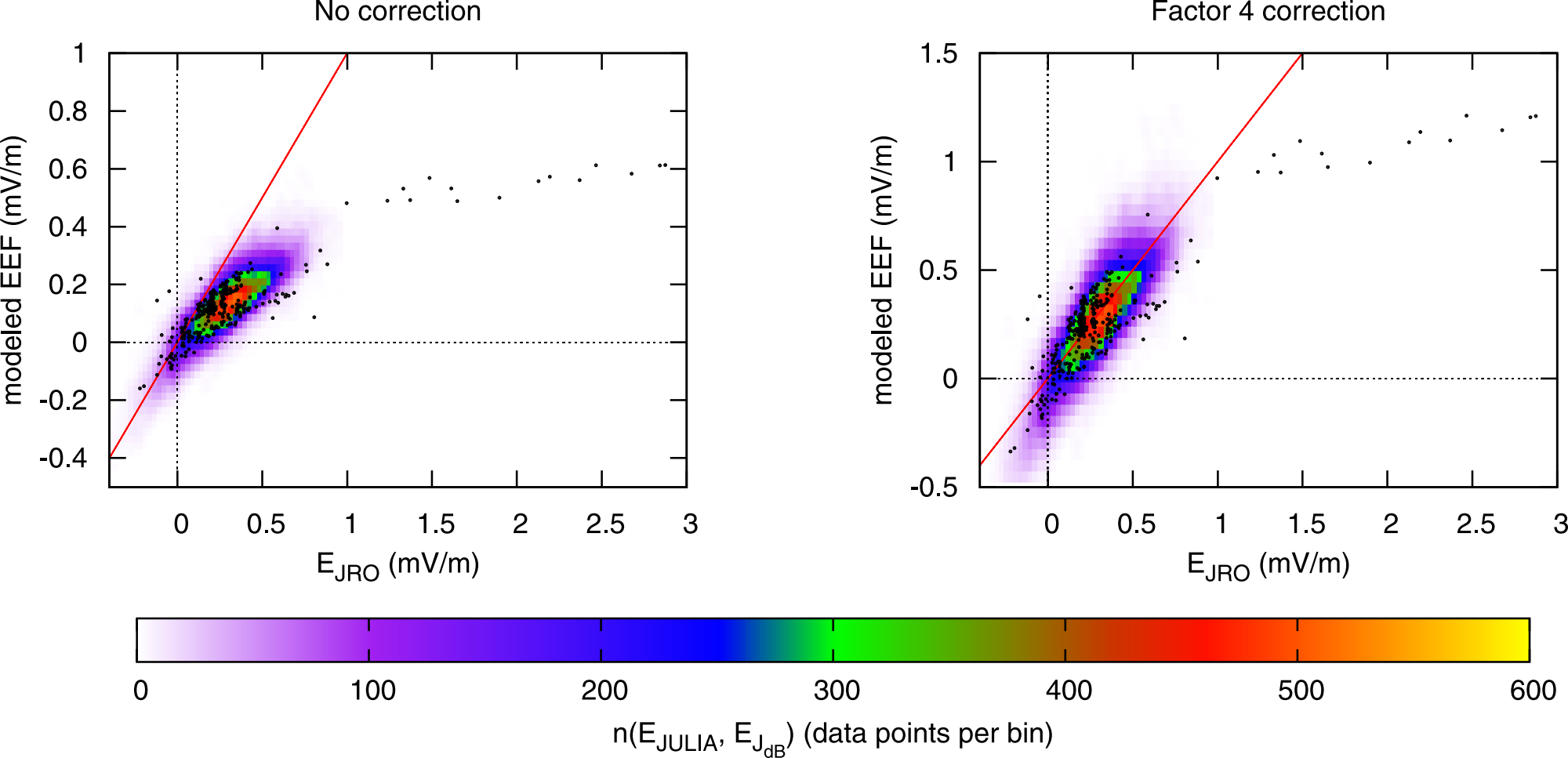
No correction
Factor 4 correction
modeled EEF (mV/m)
E_JRO (mV/m)
n(E_JULIA, E_JdB) (data points per bin)
0
100
200
300
400
500
600

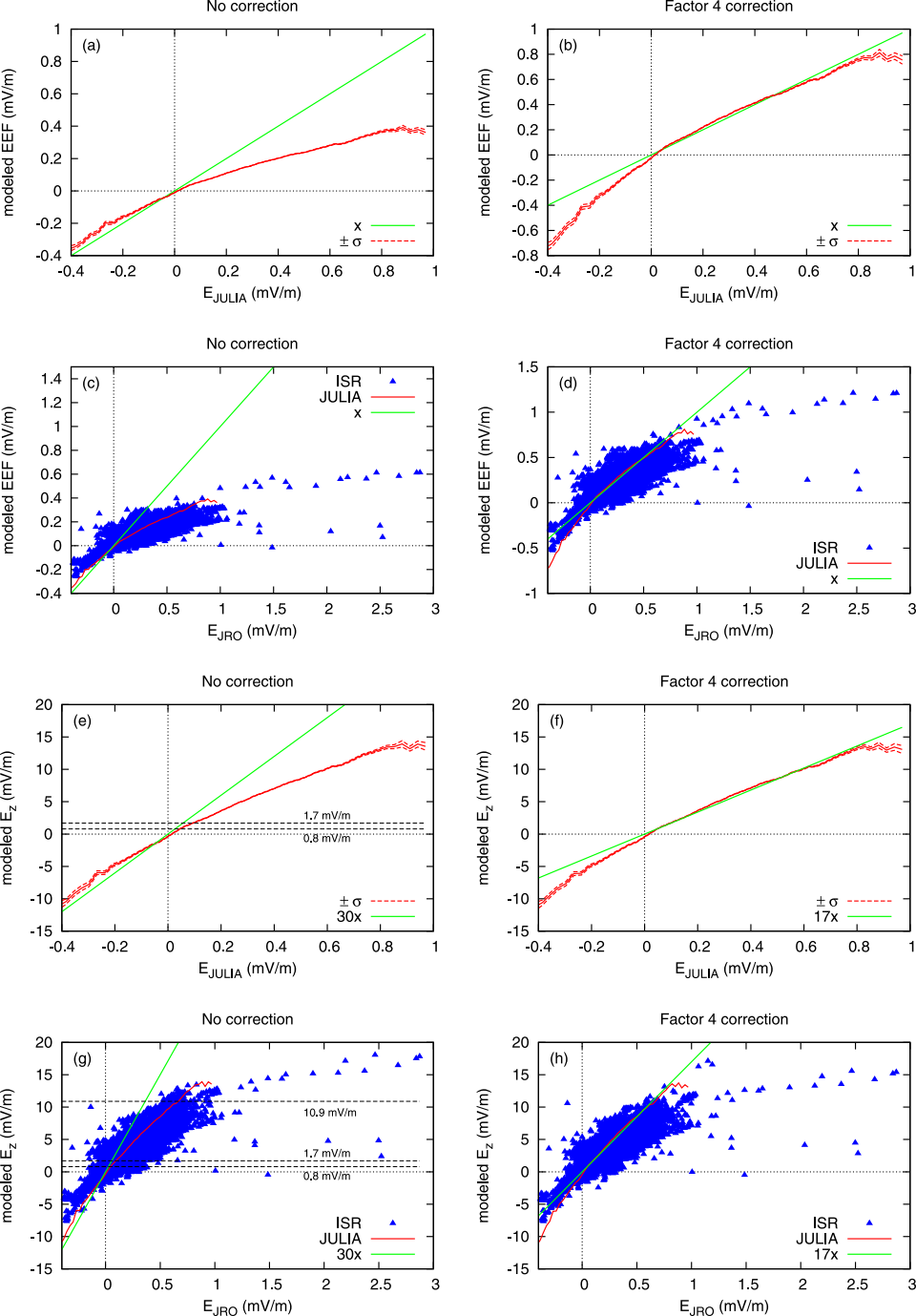
No correction
(a)
modeled EEF (mV/m)
E_JULIA (mV/m)
x
±σ
Factor 4 correction
(b)
modeled EEF (mV/m)
E_JULIA (mV/m)
x
±σ
No correction
(c)
modeled EEF (mV/m)
E_JRO (mV/m)
ISR
JULIA
x
Factor 4 correction
(d)
modeled EEF (mV/m)
E_JRO (mV/m)
ISR
JULIA
x
No correction
(e)
modeled E_Z (mV/m)
E_JULIA (mV/m)
1.7 mV/m
0.8 mV/m
±σ
30x
Factor 4 correction
(f)
modeled E_Z (mV/m)
E_JULIA (mV/m)
±σ
17x
No correction
(g)
modeled E_Z (mV/m)
E_JRO (mV/m)
10.9 mV/m
1.7 mV/m
0.8 mV/m
ISR
JULIA
30x
Factor 4 correction
(h)
modeled E_Z (mV/m)
E_JRO (mV/m)
ISR
JULIA
17x